HHS Public Access

Author manuscript

Nanomedicine. Author manuscript; available in PMC 2018 May 01.

Published in final edited form as:

Nanomedicine. 2017 May ; 13(4): 1353–1362. doi:10.1016/j.nano.2017.01.009.

Imaging the Delivery of Drug-loaded, Iron-stabilized Micelles

Dr. Suzanne J. Bakewell, Ph.D.[1,*], **Dr. Adam Carie, Ph.D.**[1], **Ms. Tara L. Costich, B.S.**[1], **Dr. Jyothi Sethuraman, Ph.D.**[1], **Dr. J. Edward Semple, Ph.D.**[1], **Dr. Bradford Sullivan, Ph.D.**[1], **Dr. Gary V. Martinez, Ph.D.**[2], **Dr. William Dominguez-Viqueira, Ph.D.**[2], and **Dr. Kevin N. Sill, Ph.D.**[1]

[1] Intezyne Technologies, 3720 Spectrum Boulevard, Suite 104, Tampa, FL, 33612

[2] Department of Cancer Imaging and Metabolism, H. Lee Moffitt Cancer Center & Research Institute, 12902 Magnolia Drive, Tampa, FL 33612

Abstract

Nanoparticle drug carriers hold potential to improve current cancer therapy by delivering payload to the tumor environment and decreasing toxic side effects. Challenges in nanotechnology drug delivery include plasma instability, site-specific delivery, and relevant biomarkers. We have developed a triblock polymer comprising a hydroxamic acid functionalized center block that chelates iron to form a stabilized micelle that physically entraps chemotherapeutic drugs in the hydrophobic core. The iron-imparted stability significantly improves the integrity of the micelle and extends circulation pharmacokinetics in plasma over that of free drug. Furthermore, the paramagnetic properties of the iron-crosslinking exhibits contrast in the tumors for imaging by magnetic resonance. Three separate nanoparticle formulations demonstrate improved anti-tumor efficacy in xenograft models and decreased toxicity. We report a stabilized polymer micelle that improves the tolerability and efficacy of chemotherapeutic drugs, and holds potential for non-invasive MRI to image drug delivery and deposition in the tumor.

Graphical abstract

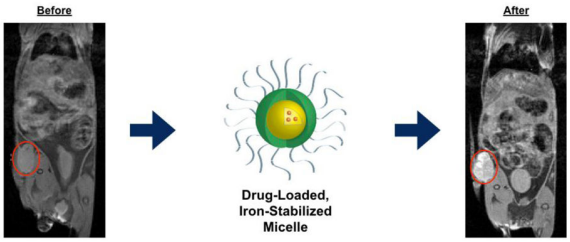

Corresponding Author: Dr. Suzanne J. Bakewell; 3720 Spectrum Blvd., Suite 104, Tampa, FL 33612; (tel) 813-910-2120 (fax) 813-354-3637; suzanne.bakewell@intezyne.com.

Conflicts of Interest: The authors have no conflict of interest to declare.

Animals with subcutaneous xenograft tumors are injected with encapsulated (non-covalently) drugs in iron-stabilized polymer micelles. At 24 hours contrast in the tumor is identified by MRI, and although signal is cleared by 168 hours, tumor growth is significantly inhibited by release of the API over time from the polymer micelle.

Keywords

Polymer micelle; chemotherapeutics; iron-stabilization; targeted delivery; MRI agent

BACKGROUND

The idealized goal for chemotherapy is to provide a highly efficacious treatment with minimal toxicity. Side effects are the result of off-target effects on healthy tissue and for this reason site-specific delivery of oncology drugs has been a decades-long goal. Nanoparticle drug carriers offer a promising solution to this goal by overcoming inherent biological barriers. Due to their unique size range (20-150 nm), nanocarriers can evade the mononuclear phagocyte system[1-3], uptake by the liver, and avoid renal clearance. Increased circulation time enhanced by micelle stability in plasma, allows nanoparticles to preferentially accumulate in solid tumors *via* the enhanced permeation and retention (EPR) effect [4, 5], thereby improving treatment efficacy [6].

Polymer micelles are assemblies of amphiphilic block copolymers forming a core-shell structure that is well suited for drug delivery, where hydrophobic molecules are segregated to the core. These 100 nm clusters of surfactant molecules are formed in water when the concentration is above the critical micelle concentration (CMC)[7, 8]. Traditional surfactant micelles are unstable below the CMC [9], so an approach to produce a stable polymer micelle typically includes crosslinking of the micelle “shell” or “core” using ester, amide, disulfide, or radical chemistries[10-15]. Polymer or liposomal self-assembly without crosslinking typically results in reduced stability in circulation and premature drug release. Core and shell stabilization has achieved varying degrees of success, but concerns remain regarding drug loading effectiveness, stability, drug release, and preparation.

A less common approach to core crosslinking involves a triblock copolymer specifically designed to address the inherent micelle instability. Triblock copolymer production incorporates a middle block in addition to the standard hydrophobic and hydrophilic blocks, which imparts micelle stability. Previously this approach was utilized with vinyl-based polymers prepared from radical polymerization techniques[16-21]. We have developed a micelle forming triblock copolymer specifically designed to address the inherent stability of nanoparticles. This polymer contains a hydroxamic acid block that can chelate with iron atoms. The addition of iron to the triblock copolymer micelle results in the formation of dative bonds among the polymer chains, providing stability at neutral pH. At low pH, such as conditions found in the tumor environment, the iron-hydroxamic bonds dissociate, reducing particle stability, and subsequently release the drug [22, 23].

Magnetic nanoparticles possess unique properties that make them an attractive contrast agent for magnetic resonance imaging[24]. Iron oxide nanoparticles such as magnetite (Fe_3O_4),

maghemite (Fe_2O_3), ferumoxides, and ferucarbotran demonstrate superparamagnetic properties [25, 26] with a mean particle diameter of approximately 50 nm and have been widely investigated for magnetic resonance imaging (MRI) application. The combination of magnetic nanoparticles, or other contrast media, with nanoparticle drug carriers have resulted in dual-purpose nanoparticles often referred to as "theranostics"[27]. This approach enables the nanoparticle platform to carry both a therapeutic agent in addition to a diagnostic agent to reveal spatial location within the patient. Approaches to theranostics include the encapsulation of iron-oxide nanoparticles in crosslinked diblock copolymers[28]; oxaliplatin and gadolinium complexes in diblock copolymer micelles[29]; and doxorubicin and iron oxide nanoparticles in folate-targeted polymer micelles[30]. Contrary to these theranostic nanoparticles that co-encapsulate the imaging agent and the drug, we have discovered that our drug-loaded hydroxamic-acid micelles inherently function as a MRI contrast agent through the clustering of the iron-stabilizing atoms.

The aim of this study was to design a stabilized polymer micelle to encapsulate hydrophobic chemotherapeutics and to improve drug delivery to tumors. Our non-covalent encapsulation of drug improved plasma pharmacokinetics, decreased systemic toxicity and increased efficacy in colorectal, lung, and fibrosarcoma tumors. Iron dative bonds that stabilize the micelle provide contrast for magnetic resonance and an additional aim of the study was to identify the tumor in subcutaneous models and in an orthotopic breast model. We further confirmed drug delivery by immunohistochemistry data in a colorectal xenograft tumor model. In this report, we demonstrate that stabilized polymer micelles accumulate in the tumor environment, reduce toxic side effects, increase anti-tumor efficacy, and provide potential for imaging biomarker applications in the clinic.

METHODS

Preparation and Physiochemical Characterization of Drug-loaded Micelle Formulations

Triblock copolymer methoxy-poly(ethylene glycol)-*block*-poly[(D-glutamic acid-*gamma*-hydroxamate)-*co*-(L-glutamic acid-*gamma*-hydroxamate)]-*block*-poly[(L-tyrosine)-*co*-(D-phenylalanine)]-acetamide and methoxy-poly(ethylene glycol)-*block*-poly[(D-glutamic acid-*gamma*-hydroxamate)-*co*-(L-glutamic acid-*gamma*-hydroxamate)]-*block*-poly[(L-tyrosine)-*co*-(D-phenylalanine)-*co*-(D-leucine)]-acetamide were prepared according to methods presented in US Patent 9,078,930. Micelle formulations were prepared using an oil-in-water emulsion technique where the polymer was dissolved in the aqueous phase and the drug dissolved in the organic phase. The components were combined while mixing under high shear to form an emulsion with minimal droplet size. Removal of the organic phase induced micelles self-assembly resulting in drug encapsulation. Iron was added to stabilize the formulations, and further purification and concentration was done by tangential flow filtration. Cryoprotectant was added, the formulations were filtered using a 0.22 μm filter, and lyophilized to dryness. Potency of the formulations was determined by HPLC/UV and represented as weight loading as a percentage of drug to total formulation weight (% w/w). Average particle diameter and particle size distribution (D10/50/90) were determined using dynamic light scattering (DLS).

Plasma Pharmacokinetics in the Cannulated Rat Model

Female Sprague-Dawley rats surgically modified with jugular vein catheters (JVC) (Envigo, Indianapolis, IN, USA) were used to determine the pharmacokinetics of micelle formulations compared to free drug. The Institutional Animal Care and Use Committee (IACUC), at the University of South Florida (USF) approved all rat *in vivo* study protocols. Animals were maintained and evaluated under pathogen-free conditions in accordance with USF College of Medicine IACUC standards of care. Test articles were reconstituted in 0.9% saline for injection at concentrations equivalent to the free drug administered on a mg/kg basis (adjusted for formulation weight loading), and were administered by fast bolus to the JVC followed by saline flush. Blood was collected into tubes containing K_2EDTA, centrifuged to isolate plasma, and frozen until processed for HPLC analysis. Catheters were maintained by heparinized saline flush after blood collection. Plasma samples were processed by protein precipitation for drug recovery, followed by HPLC separation and detection by fluorescence. This methodology was used to detect total drug concentration in the plasma, and is not capable of discriminating between encapsulated and unencapsulated forms for micelle test articles. Standard curves were prepared in blank rat plasma, with peak integration and curve fits performed by Empower (Waters, Milford, MA, USA). Noncompartmental analysis of pharmacokinetic parameters was performed using Phoenix WinNonlin version 6.3 (Pharsight, Princeton, NJ, USA).

Transmission Electron Microscopy

IT-141 and IT-147 micelle formulations were reconstituted in dH_2O at a concentration of 16 mg/mL. 200 μL of reconstituted IT-141 was placed in a carbon-coated formvar grid at 4°C. After evaporation of the solute, a drop of 1% osmium tetroxide in dH_2O at 4°C was placed on the sample and allowed to evaporate in a fume hood on ice packs. For IT-147 TEM images, 5 μL of the reconstituted formulation was dropped onto a FCF440 mesh copper grid, wicked and air dried before staining with 1% uranyl acetate. Grids were imaged and photographed at 60 kV in an FI Morgagni TEM (FI, Inc., Hillsboro, OR), using an Olympus MegaView III digital camera.

Cell Culture

HCT116 colorectal carcinoma (no. CCL-247), HT1080 fibrosarcoma (no. CCL-121), HT-29 colorectal adenocarcinoma (no. HTB-38), MCF-7 breast adenocarcinoma (no. HTB-22), and A549 (no. CCL-185) and NCI-H460 (no. HTB-177) lung carcinomas were all purchased from ATCC (Manassas, VA, USA) and maintained in appropriate growth media. ATCC uses morphology, karyotyping, and PCR based approaches to confirm the identity of human cell lines and to rule out both intra- and interspecies contamination. These include an assay to detect species specific variants of the cytochrome C oxidase I gene (COI analysis) to rule out inter-species contamination and short tandem repeat (STR) profiling to distinguish between individual human cell lines and to rule out intra-species contamination. All cell lines were used within 2 months of receipt or resuscitation from ATCC. For tumor inoculation, cells were trypsinized when at 80-90% confluency and at low passage number.

In Vivo Efficacy

The Institutional Animal Care and Use Committee, at the University of South Florida approved all *in vivo* study protocols. Data collection methods were predetermined, and animals were assigned randomly to treatment groups. 6-Week old female, athymic nude mice (Charles River Laboratories, Wilmington, MA, USA) were maintained in pathogen-free conditions in accordance with the University of South Florida IACUC standards of care. The mice were given food and water ad libitum. Mice were euthanized if tumors ulcerated, impeded mobility, or affected general health. Depending on study model, animals were inoculated with 2×10^6 – 5×10^6 cells in a 100 μL bolus injection. Cells were implanted subcutaneously on the right flank of each mouse. Test articles were administered by fast bolus to the mouse tail vein once tumors reached a volume greater than 100 mm^3. Tumors were measured bi-dimensionally three times per week with electronic calipers using LabCat In-Life Module software (Innovative Programming Associates, Inc. Lawrenceville, NJ, USA). Tumor volume was calculated in the LabCat program according to the formula:

$$\mathrm{V}=\frac{(\text{short}\quad\text{diameter})^2\times(\text{long}\quad\text{diameter})}{2}$$

Percent tumor growth inhibition was calculated according to the formula:

$$\%\quad\mathrm{TGI}=\left(1-\left(\frac{\mathrm{V_{tf}}-\mathrm{V_{ti}}}{\mathrm{V_{cf}}-\mathrm{V_{ci}}}\right)\right)\times100$$

where V_{tf} is the volume of the treatment group on the final measurement day, V_{ti} is the volume of the treatment group on D0, V_{cf} is the volume of the formulation control group on the final measurement day, and V_{ci} is the volume of the formulation control group on D0. Percent tumor regression was calculated according to the formula:

$$\%\quad\mathrm{Regression}=\left(\frac{\mathrm{V_i}-\mathrm{V_f}}{\mathrm{V_i}}\right)\times100$$

where V_i is the volume on the final measurement day and V_f is the volume on D0.

In Vivo Toxicity

Animals were monitored daily and gross observations were recorded throughout the study. Gross toxicity observations in response to dosing of the free drug at the MTD were recorded and were consistent with published observed gross toxicities. When gross toxicities were observed in the corresponding API micelle formulation groups that dose was recorded as the MTD of the formulation. Weights were recorded 3 times weekly and any animals that lost more than 20% of their starting body weight were removed from the study and monitored until body weight recovered.

Immunohistochemistry Analysis

All in vitro studies were performed from a minimum of three experimental replicates. Staining was performed on formalin-fixed paraffin embedded tumor sections (3-5 μm) using the Vectastain elite avidin-biotin complex kit (Vector Laboratories, Burlingame, CA, USA). Briefly, after antigen retrieval with 10 mM sodium citrate (pH 6.5) paraffin sections were incubated with rabbit anti-γ-H2AX monoclonal antibody (Ser139) (Novus Biologicals, Littleton, CO) in blocking solution (1% serum in PBS plus 0.4% Triton X-100, ABC Elite Kit, Vector Laboratories) at 4ºC overnight. All sections were processed with the ABC Elite Kit (Vector Laboratories) per manufacturer's recommendation. The immunoreactivity was visualized using peroxidase-DAB (3,3′-diaminobenzidine). All sections were counterstained with Mayer's hematoxylin, dehydrated and cover slipped. Negative controls with no primary antibody were used to assess nonspecific staining. Two tumors per time point, a minimum of three sections per tumor and 20 fields per section were quantified.

MRI Experiments

All the experiments were performed on a 7T horizontal magnet (ASR 310, Agilent Technologies, Inc., Santa Clara, CA, USA) with 205/120/HDS gradients and 310 mm bore, using a 72 mm ID birdcage RF-coil (Agilent Technologies, Inc.) for in vitro experiments and a 35-mm Litzcage RF-coil (Doty Scientific, Inc., Columbia, SC, USA) for *in vivo* experiments at the Small Animal Imaging Laboratory, Moffitt Cancer Center, Tampa, FL, supported by 5P30-CA076292.

In Vitro MRI Analysis

Multiple concentrations of each nanoparticle were prepared at values ranging from 0.002 mM to 0.6 mM and repeated in triplicate in a 96-well plate cut into two. Spin echo imaging sequences were used with either multiple TR values (Progressive Saturation) or followed by a train of 180° pulses for collection of multiple spin echoes (MEMS) to estimate spin-lattice (R_1) and spin-spin (R_2) relaxation rate constants respectively. Images were collected with a field of view of 8 × 4 cm^2 and a matrix size of 256 × 128 pixels. Signal mean values were obtained from regions of interest within each well and used to obtain the relaxation rates with a nonlinear least squares fit using the Levenberg-Marquardt algorithm. Subsequently estimates of the each relaxivity parameter (n = 1 for spin lattice or n = 2 for spin-spin) were determined by linear regression of the expression $r_n = (R_n - R_{n,0}) / [\text{nanoparticle}]$, where R_n refers to relaxation rate constant R_1 or R_2.

In Vivo MRI Analysis

Xenograft tumor bearing mice were injected *via* the lateral tail vein with formulation reconstituted in saline. During imaging mice were continuously anesthetized with 2% isofluorane delivered using a nose count mounted on the mouse holder. Whole body coronal slices were acquired using a multislice spin-echo (SEMS) sequence with TR/TE 315/7.43ms, 17 slices, 1 mm slice thickness and 2 averages, FOV = 80 × 40 mm 256 × 128 pixels. Axial images were acquired with FOV = 40 × 40 mm^2, 128 × 128 pixels using the same multislice spin-echo sequence TR/TE 315/7.43ms, 17 slices, 1 mm slice thickness, 2

averages. Images were acquired before drug injection, and again at multiple time points thereafter to monitor drug delivery and clearance.

Statistical Analysis

Statistical analyses were performed using GraphPad Prism (GraphPad Software, Inc., La Jolla, CA, USA). Plotted values represent means ± SEM. For *in vivo* studies, a Student's *t* test was performed to assess the statistical significance of tumor volume differences between treated and formulation control groups. *P* values of ≤ . 5 were considered statistically significant.

RESULTS

We have prepared a triblock copolymer comprised of a poly(ethylene) glycol (PEG) hydrophilic block, a central glutamic acid hydroxamate stabilizing block, and a hydrophobic polypeptide block (Figure 1). The hydroxamic acid-containing block interacts with iron atoms to form dative bonds among the polymer chains to stabilize the micelle. Iron chelation imparts transient stability to the nanoparticle in neutral pH environments. These iron-hydroxamic acid dative bonds are unstable at low pH, providing a mechanism for environment-dependent micelle stability and subsequent drug release (Supplementary Figure 1). Application of our technology has produced formulations of stable micelles that encapsulate hydrophobic anticancer agents to include SN-38, daunorubicin, epothilone D, panobinostat, paclitaxel, and aminopterin (Table 1). In all cases, loading active pharmaceutical ingredient (API) averaged more than 80% efficiency with API weight loading ranging from 3.0%-7.4% (w/w) from 4%-10% feed (w/w), respectively. Average micelle diameters range between 58-120 nm as verified by electron microscopy (TEM) and by dynamic light scattering (Figure 2, Supplementary Figure 2). In this report, we will discuss data with polymer micelles encapsulating the following: SN-38 (IT-141), daunorubicin (IT-143), and epothilone D (IT-147).

A direct measure of the stability imparted by the iron-chelated center block to the polymer micelles can be probed using pharmacokinetic (PK) studies. Studies were conducted in rats that compared the PK of the free drug unencapsulated, to a drug-loaded micelle prepared with a triblock copolymer *without* iron, and an iron-stabilized micelle formulation of the drug. The area under the concentration-time curve (AUC), or plasma exposure, was significantly higher (ca. 600-fold increase) for the iron-stabilized micelles. For example, with the nanoparticle formulation of daunorubicin (IT-143) we found the plasma exposure to be 0.96 and 1.5 μg*h/mL for the free drug and unstabilized micelle, respectively, while an AUC of 913.7 μg*h/mL was obtained for the iron-stabilized formulation (Figure 3). These results indicate that our iron-stabilized micelles are stable to dilution in the blood compartment following systemic administration.

Based upon the use of iron as a stabilization agent, we investigated whether our iron-stabilized micelles would exhibit superparamagnetic or paramagnetic behavior. To evaluate the possibility of these nanoparticles providing magnetic resonance contrast, we began with phantom MR relaxivity studies. Experiments were conducted on iron-stabilized micelles and revealed spin-lattice relaxivity values (r_1) of 7-16 $mM^{-1}s^{-1}$ and spin-spin relaxivity values

of 36-53 $mM^{-1}s^{-1}$ (Supplementary Figure 3). Control phantom experiments with iron(III) acetylacetonate did not provide any measurable magnetic resonance contrast. These results suggested that *in vivo* magnetic resonance imaging of these iron-stabilized nanoparticles was plausible, and that a standard T_1-weighted sequence could be used to observe enhancement within the tumor.

We investigated time-course positive MRI contrast from our crosslinked nanoparticles in four subcutaneous *in vivo* xenograft tumor models (HT-29, HCT116, A549, NCI-H460) and one breast orthotopic model (MCF-7) (n=20). In an HCT116 mouse xenograft model post-administration of an SN-38-loaded, iron-stabilized micelle (IT-141) shows contrast from the intact, iron-containing nanoparticles in the subcutaneous tumor, peaking between 24 and 48 hours (n=4) (Figure 4A). The signal is cleared at 168 hours (Figure 4B). MRI was repeated with IT-141 in HT-29 colorectal (n=3) and A549 lung (n=4) subcutaneous tumor models (Supplementary Figure 4A and 4B). These results were replicated with the epothilone D-loaded, iron-stabilized micelle (IT-147), and contrast imaging performed over time in subcutaneous xenograft models HCT116 colorectal (n=3) (Figure 4C) and NCI-H460 lung (n=3) (Figure 4D), and in an MCF-7 breast orthotopic (n=5) (Supplementary Figure 4C) tumor models. These experiments demonstrate that intact iron-stabilized micelles accumulate in the tumor environment and provide sufficient contrast in MR imaging useful for theranostic applications. Positive magnetic resonance contrast of these nanoparticles should allow for imaging biomarker applications in the clinic, as we envision the potential ability to screen patients based upon enhanced magnetic resonance signal in the tumor.

As with all drugs in development for oncology applications, efficacy with predictable toxicity is paramount. *In vivo* efficacy of our stabilized nanoparticle formulations was demonstrated in HT-29, HCT116, NCI-H460, and A549 xenograft models (Table 2). SN-38 loaded, iron-stabilized micelles (IT-141) were evaluated in an HCT116 xenograft models and compared to irinotecan treatment. SN-38 is the active metabolite of irinotecan and cannot be administered systemically due to its poor solubility. In the HCT116 model, three weekly doses of 50 mg/kg saw an average tumor regression of 48%, compared to the formulation control group (Figure 5A). The 50 mg/kg irinotecan dosed group in our model showed a 70% tumor growth inhibition. Following three weekly intravenous doses in the HT-29 model, we observed 64% and 98% tumor growth inhibition in the 40 mg/kg and 60 mg/kg treated groups (IT-141) compared to the formulation control group (Figure 5B). The equitoxic dose of 17.5 mg/kg inhibited tumor volume growth by 97%. In the A549 lung model encapsulation of epothilone D, a potent in vitro cytotoxin with IC50s in the nanomolar range, raised the MTD of free drug from 5 mg/kg to 30 mg/kg and the average tumor growth inhibition from 2% to 46%. In the HCT116 model (Figure 5C) tumor volume growth was inhibited by 38% in the free drug group compared to 87% in the IT-147 group.

In all cases, when the micelle formulation is dosed at the MTD of the free drug we eliminate the gross toxicities observed in the free drug cohort. Body weights were recorded throughout the efficacy studies to quantify toxicity effects and at no point in the studies did the weights drop below 20% of the starting weight (Figures 5D, 5E, 5F). Animals in all groups survived treatment. Furthermore, tail necrosis from the bolus injection in the IT-143 treated animals, compared to the daunorubicin free drug treated animals, was significantly decreased,

suggesting successful encapsulation of the anthracycline and protection from vesicant extravasation.

To confirm that the encapsulated drug is responsible for anti-tumor activity, we investigated the incidence of double stranded breaks by γ-H2AX expression in tumors treated with SN-38 loaded, iron-stabilized micelles (IT-141), compared to irinotecan treatment at different time points (4, 48, 7 , and 44 hours). n irinotecan treated tumors, γ-H2AX expression peaked at 72 hours followed by a sharp decrease in expression at 144 hours. In IT-4 treated tumors, γ-H2AX positive staining increased steadily from 24 through 144 hours (Figures 6A and 6B). This shift in the kinetics of the SN-38 pharmacodynamics corroborates the biodistribution studies where IT-141 delivered a minimum of 11-fold more SN-38 to the tumor compared to irinotecan (Figure 6C). Our DNA damage assay demonstrates that IT-141 extends the pharmacodynamic effect over irinotecan in treated tumors.

DISCUSSION

There remain numerous cancer drug molecules that are highly hydrophobic and require improvements in delivery. Many currently require immunogenic excipients for administration such as polyethylated castor oil, resulting in patients enduring long infusion rates and mandatory co-administration of anti-inflammatories and antihistamines. Nanomedicine overrides this step, as nab-paclitaxel has shown. However, nab-paclitaxel does not fundamentally change the pharmacokinetics over taxol, but does improve the toxicity profile. [31] Similarly, a high number of polymer nanoparticles are unstable after injection into the bloodstream. Polymer micelles, a subset of polymer nanoparticles, exist in solution as a dynamic mixture of assembled micelles and polymer unimers. The equilibrium between the two species is generally dictated by polymer concentration. As the concentration falls (e.g. dilution in the blood stream) the population of unimers is increased and the number of micelles correspondingly decreases. To address this inherent instability, we designed a micelle that is stabilized by the chelation of iron atoms. In our micelles, crosslinking the center block of the polymers with iron atoms effectively binds the micelle chains together, imparting stability to the micelle that is independent of concentration changes. We have demonstrated herein that the iron stabilization extends the circulation time of encapsulated drugs without chemical conjugation. Careful selection of the hydrophobic polypeptide block has allowed us to successfully entrap a wide range of hydrophobic drugs. As a covalent bond between the drug and the polymer is not required to encapsulate the drug in our formulation, it avoids the cleavage step required by many drug delivery systems. [32] Similarly, irinotecan is the prodrug of SN-38 and requires cleavage by carboxylesterase to release the active metabolite. There are patients that have a diminished response to irinotecan therapy because of impaired enzyme activity which affects the overall metabolic efficacy results in the clinic. [33, 34] Drug concentrations in biological media discussed herein represent the sum of both free and encapsulated drug, as analytical techniques to differentiate between free and micelle encapsulated drug have yet to be developed. Although our micelles do not covalently entrap the hydrophobic drug, the release rate of the drug from the micelle and the ratio of diffused versus entrapped drug are currently under investigation. With no enzymatic activity to quantify the release of the API, the challenge is to differentiate

between entrapped versus free drug in circulation. [35] The improved PK, MRI, and efficacy data suggest that the drug is successfully encapsulated and transported to the target tissue.

Our stabilized polymer micelle not only has an improved pharmacokinetic profile over free drug, but also has increased biodistribution when we measure drug concentrations in tumor tissues. The physiological pH of evaluated organs is constant and it is hypothesized that the polymer micelles are intact and do not release drug in physiological pH as toxicity is not observed at equivalent doses. With some formulations (for example IT-147[22]), we can dose as high as 6-fold over the free drug MTD before we observe comparable toxicity (such as neurotoxicity with IT-147). The stabilization leads to accumulation (as a consequence of the leaky nature and poor drainage of the tumor vasculature) at the target site where we hypothesize that the lower pH of the tumor microenvironment causes disintegration of the iron crosslinking bonds and delivery of the drug. Studies with IT-141 to evaluate double-stranded DNA breaks in tumor tissue confirms that SN-38 is delivered to the tumor, and kinetics of the pharmacodynamic response are extended by the stabilized micelle formulation when compared to irinotecan. Studies are underway to determine the duration of this effect as seen with the formulation dosing. It is our premise that our iron-stabilized micelles behave as a MR contrast agent because the stability-providing spherical shell of iron atoms gives the micelles inherent paramagnetic or superparamagnetic properties. This unique attribute results in the ability to image these nanoparticles *in vivo* by T_1-weighted MRI. Given sufficiently modest T_2-effects, all paramagnetic or superparamagnetic nanoparticles will display positive enhancement. The relaxivity values obtained for our iron-stabilized micelles are similar to the relaxivity values for circa 15 nm iron oxide nanoparticles. [36] These relaxivities were favorable to achieve T_1-weighted imaging with a standard spin echo pulse-sequence, whereas many applications with magnetic nanoparticles are achieved with T_2 or T^{2*}-(negative) contrast. These results hold potential for use in the clinic where delivery of the chemotherapeutic-loaded nanoparticles can be monitored non-invasively, and where patients may be selected based upon sufficient nanoparticle uptake by the tumor.

Drug-loaded, iron-stabilized micelles demonstrate altered biodistribution and clearance kinetics in animal models, with an observed increase in anti-tumor efficacy and decrease in toxicity. Therefore, we have shown an example of nanotechnology that not only improves delivery and therapeutic outcome, but also holds potential for enhanced patient quality of life.

Supplementary Material

Refer to Web version on PubMed Central for supplementary material.

Acknowledgments

Funding: Research reported in this publication was supported by the National Cancer Institute of the National Institutes of Health under Award Number U43CA179468 and under Contract No. HHSN261201400018C.

REFERENCES

1. Torchilin VP. Multifunctional nanocarriers. Adv Drug Deliv Rev. 2006; 58:1532–55. [PubMed: 17092599]
2. Lammers T, Kiessling F, Hennink WE, Storm G. Drug targeting to tumors: Principles, pitfalls and (pre-) clinical progress. J Control Release. 2012; 161:175–87. [PubMed: 21945285]
3. Cho K, Wang X, Nie S, Chen ZG, Shin DM. Therapeutic nanoparticles for drug delivery in cancer. Clin Cancer Res. 2008; 14:1310–6. [PubMed: 18316549]
4. Maeda H, Wu J, Sawa T, Matsumura Y, Hori K. Tumor vascular permeability and the epr effect in macromolecular therapeutics: A review. J Control Release. 2000; 65:271–84. [PubMed: 10699287]
5. Maeda H, Sawa T, Konno T. Mechanism of tumor-targeted delivery of macromolecular drugs, including the epr effect in solid tumor and clinical overview of the prototype polymeric drug smancs. J Control Release. 2001; 74:47–61. [PubMed: 11489482]
6. Arruebo M, Fernández-Pacheco R, Ibarra MR, Santamaría J. Magnetic nanoparticles for drug delivery. Nano Today. 2007; 2:22–32.
7. Dominguez A, Fernandez A, Gonzalez N, Iglesias E, Montenegro L. Determination of critical micelle concentration of some surfactants by three techniques. Journal of Chemical Education. 1997; 74:1227–31.
8. Kile DE, Chiou CT. Water solubility enhancements of ddt and trichlorobenzene by some surfactants below and above the critical micelle concentration. Environ Sci Technol. 1989; 23:832–38.
9. Savic R, Eisenberg A, Maysinger D. Block copolymer micelles as delivery vehicles of hydrophobic drugs: Micelle-cell interactions. J Drug Target. 2006; 14:343–55. [PubMed: 17092835]
10. Kataoka K, Harada A, Nagasaki Y. Block copolymer micelles for drug delivery: Design, characterization and biological significance. Advanced Drug Delivery Reviews. 2012; 64:37–48.
11. McCormick CL, Lokitz BS, Li Y. Synthesis of reversible shell crosslinked nanostructures. United States. 2008
12. Becker ML, Bailey LO, Wooley KL. Peptide-derivatized shell-cross-linked nanoparticles. 2. Biocompatibility evaluation. Bioconjug Chem. 2004; 15:710–7. [PubMed: 15264857]
13. Crielaard BJ, Rijcken CJF, Quan L, van der Wal S, Altintas I, van der Pot M, et al. Glucocorticoid-loaded core-cross-linked polymeric micelles with tailorable release kinetics for targeted therapy of rheumatoid arthritis. Angew Chem Int Ed Engl. 2012; 124:7366–70.
14. Kabanov AV, Alakov VY, Vinogradov S. Polynucleotide compositions. 2003
15. Knop K, Hoogenboom R, Fischer D, Schubert US. Poly(ethylene glycol) in drug delivery: Pros and cons as well as potential alternatives. Angew Chem Int Ed Engl. 2010; 49:6288–308. [PubMed: 20648499]
16. Murthy N, Campbell J, Fausto N, Hoffman AS, Stayton PS. Bioinspired ph-responsive polymers for the intracellular delivery of biomolecular drugs. Bioconjugate Chem. 2003; 14:412–19.
17. Roy D, Berguig GY, Ghosn B, Lane DD, Braswell S, Stayton PS, et al. Synthesis and characterization of transferrin-targeted chemotherapeutic delivery systems prepared via raft copolymerization of high molecular weight peg macromonomers. Polymer Chemistry. 2014; 5:1791. [PubMed: 25221630]
18. El-Sayed ME, Hoffman AS, Stayton PS. Rational design of composition and activity correlations for ph-sensitive and glutathione-reactive polymer therapeutics. J Control Release. 2005; 101:47–58. [PubMed: 15588893]
19. Li Y, Lokitz BS, McCormick CL. Raft synthesis of a thermally responsive abc triblock copolymer incorporating n-acryloxysuccinimide for facile in situ formation of shell cross-linked micelles in aqueous media,ä†. Macromolecules. 2005; 39:81–89.
20. Li Y, Lokitz BS, Armes SP, McCormick CL. Synthesis of reversible shell cross-linked micelles for controlled release of bioactive agents. Macromolecules. 2006; 39:2726–28.
21. Nystrom AM, Bartels JW, Du W, Wooley KL. Perfluorocarbon-loaded shell crosslinked knedel-like nanoparticles: Lessons regarding polymer mobility and self assembly. Journal of polymer science Part A, Polymer chemistry. 2009; 47:1023–37.

22. Carie A, Sullivan B, Ellis T, Semple JE, Buley T, Costich TL, et al. Stabilized polymer micelles for the development of it-147, an epothilone d drug-loaded formulation. Journal of drug delivery. 2016; 2016:1–12.
23. Costich TL, Carie A, Semple JE, Sullivan B, Vojkovsky T, Ellis T, et al. It-143, a polymer micelle nanoparticle, widens therapeutic windows of daunorubicin. Pharmaceutical Nanotechnology. 2016; 4:3–15.
24. Sun C, Lee JS, Zhang M. Magnetic nanoparticles in mr imaging and drug delivery. Adv Drug Deliv Rev. 2008; 60:1252–65. [PubMed: 18558452]
25. Corot C, Warlin D. Superparamagnetic iron oxide nanoparticles for mri: Contrast media pharmaceutical company r&d perspective. Wiley interdisciplinary reviews Nanomedicine and nanobiotechnology. 2013; 5:411–22. [PubMed: 23633290]
26. Wang YX. Superparamagnetic iron oxide based mri contrast agents: Current status of clinical application. Quant Imaging Med Surg. 2011; 1:35–40. [PubMed: 23256052]
27. Xie J, Lee S, Chen X. Nanoparticle-based theranostic agents. Adv Drug Deliv Rev. 2010; 62:1064–79. [PubMed: 20691229]
28. Kim B, Qiu J, Wang J, Taton T. Magnetomicelles: Composite nanostructures from magnetic nanoparticles and cross-linked amphiphilic block copolymers. Nano Lett. 2005; 5:1987–91. [PubMed: 16218723]
29. Vinh NQ, Naka S, Cabral H, Murayama H, Kaida S, Kataoka K, et al. Mri-detectable polymeric micelles incorporating platinum anticancer drugs enhance survival in an advanced hepatocellular carcinoma model. Int J Nanomedicine. 2015; 10:4137–47. [PubMed: 26203241]
30. Ao L, Wang B, Liu P, Huang L, Yue C, Gao D, et al. A folate-integrated magnetic polymer micelle for mri and dual targeted drug delivery. Nanoscale. 2014; 6:10710–6. [PubMed: 25096971]
31. Denes AR, Somers EB, Wong ACL, Denes F. 12-crown-4–ether and tri(ethylene glycol) dimethyl–ether plasma-coated stainless steel surfaces and their ability to reduce bacterial biofilm deposition. Journal of Applied Polymer Science. 2000; 81:3425–38.
32. Larson N, Ghandehari H. Polymeric conjugates for drug delivery. Chemistry of materials : a publication of the American Chemical Society. 2012; 24:840–53. [PubMed: 22707853]
33. Sanghani SP, Quinney SK, Fredenburg TB, Sun Z, Davis WI, Murry DJ, et al. Carboxylesterases expressed in human colon tumor tissue and their role in cpt-11 hydrolysis. Clin Cancer Res. 2003; 9:4983–91. [PubMed: 14581373]
34. Silvestris N, Simone G, Partipilo G, Scarpi E, Lorusso V, Brunetti AE, et al. Ces2, abcg2, ts and topo-i primary and synchronous metastasis expression and clinical outcome in metastatic colorectal cancer patients treated with first-line folfiri regimen. International journal of molecular sciences. 2014; 15:15767–77. [PubMed: 25198900]
35. Skoczen S, McNeil SE, Stern ST. Stable isotope method to measure drug release from nanomedicines. J Control Release. 2015; 220:169–74. [PubMed: 26596375]
36. Meyer T, Quinto C, Bao G. Controlling iron oxide nanoparticle clustering using dual solvent exchange coating method. IEEE Magnetics Letters. 2016; 7:1–4.

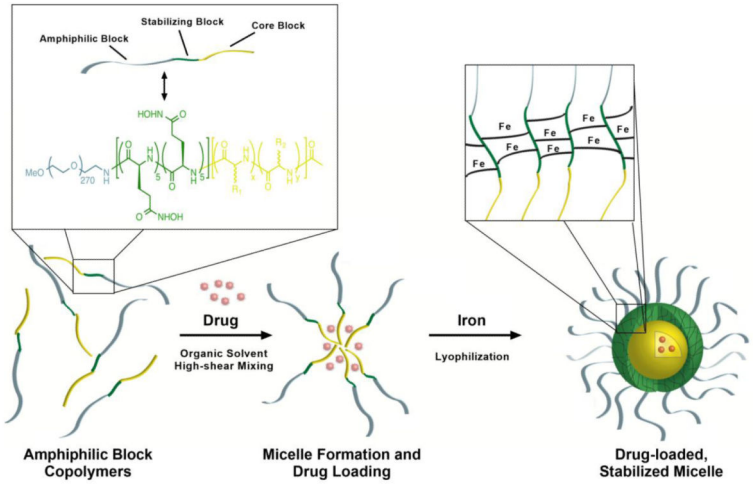

Figure 1.

Drug-loaded, iron-stabilized micelles self-assemble during formulation to form nanoparticles composed of an amphiphilic poly(ethylene glycol) corona, hydroxamic acid stabilizing middle block, and hydrophobic core block for drug encapsulation. Hydrophobic amino acids sequester drugs in the core of the micelle without the need for covalent attachment which requires chemical or enzymatic cleavage for release. Iron chelates with the hydroxamic acid moieties forming dative bonds among polymer strands to stabilize the micelle for intravenous administration and subsequent dilution. The final drug product is a lyophilized powder for reconstitution in saline for administration.

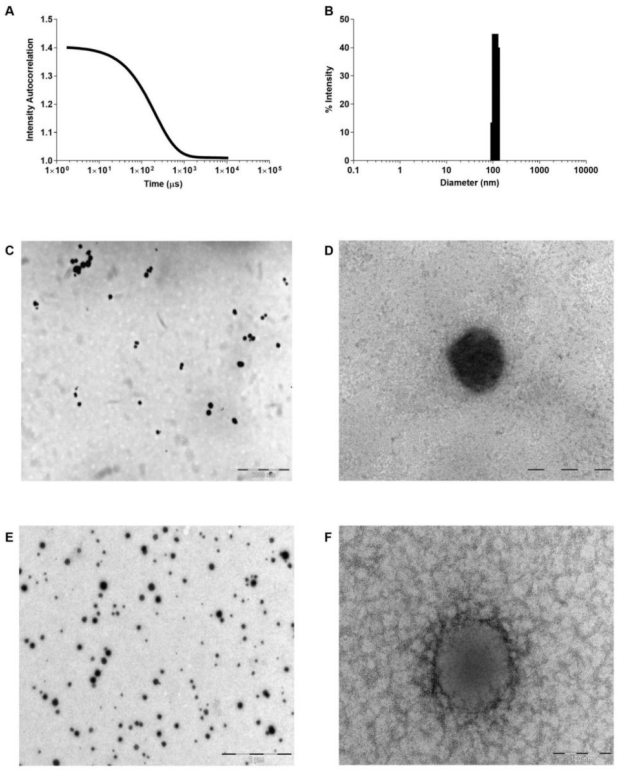

Figure 2.

Drug-loaded, iron stabilized micelles average 100 nm in diameter. (A) DLS Correlation Function Graph representing IT-141 micelle, and (B) histogram showing diameter range of IT-141 micelle. (C, D) Low and high-mag TEM image of IT-141 micelle stained with 1% osmium tetroxide. (E,F) Low and high-mag TEM image of IT-147 micelle stained with 1% uranyl acetate.

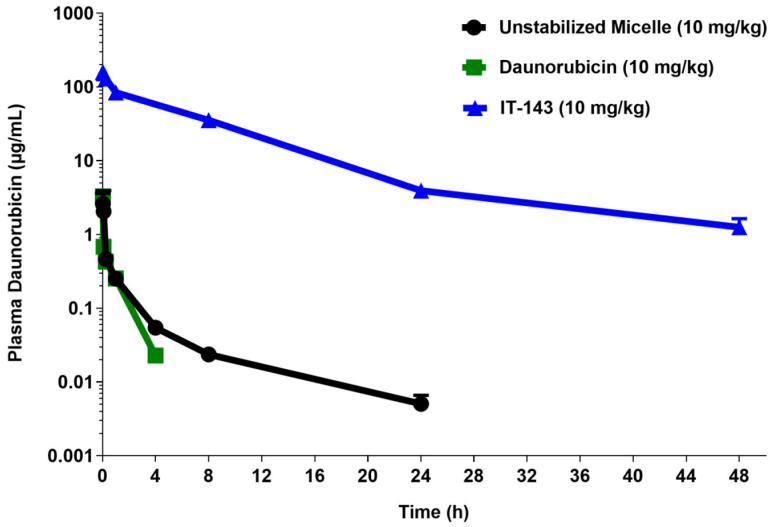

Figure 3.

Daunorubicin-loaded, iron-stabilized micelle formulation (IT-143) demonstrates prolonged circulation compared to unstabilized micelle formulation and free drug in a cannulated rat model. Intravenous administration of IT-143 resulted in exposure to the plasma compartment ($AUC_{0\text{-}48h}$) of 913.7 µg*h/mL compared to 1.5 and 0.96 µg*h/mL for unstabilized micelle formulation and daunorubicin free drug, respectively.

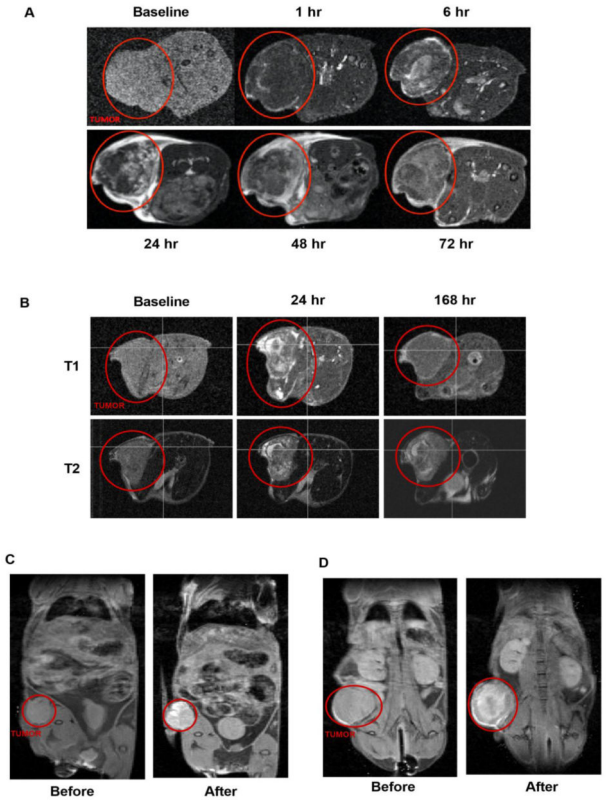

Figure 4.

MR imaging of iron-stabilized micelles in mouse subcutaneous xenograft models. (A) Time-course T_1-weighted MRI of HCT116 mouse xenograft following IV administration of SN-38-loaded, iron-stabilized micelle formulation (IT-141). Tumor is identified by red circle in both panel (A) and (B). Signal peaks around 24-48 hours and is mainly cleared by 168 hours (B). Time-course T_1-weighted MRI compared to T_2-weighted MRI in HCT116 xenograft model. Pre-dose and 48 hours MRI image of HCT116 (C) and NCI-H460 (D) mouse xenograft following IV administration of epothilone D-loaded, iron-stabilized micelle formulation (IT-147).

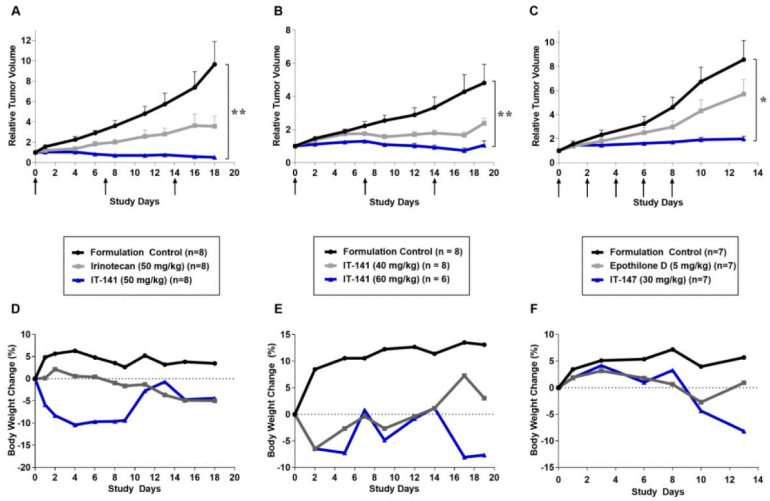

Figure 5.

Drug-loaded, iron-stabilized micelles increase anti-tumor efficacy compared to free drug in subcutaneous xenograft models. Body weights do not change more than 20% from starting weight in efficacy studies. Relative tumor volume in HCT116 colorectal model treated with IT-141 compared to irinotecan (A), HT-29 colorectal adenocarcinoma model treated with IT-141 (B), and HCT116 colorectal model treated with IT-147 (C). Arrows indicate dosing days. (D, E, F) Percent body weight change during HCT116 efficacy study using IT-141 (D), HT-29 efficacy study using IT-141 (E), and HCT116 efficacy study using IT-147 (F).

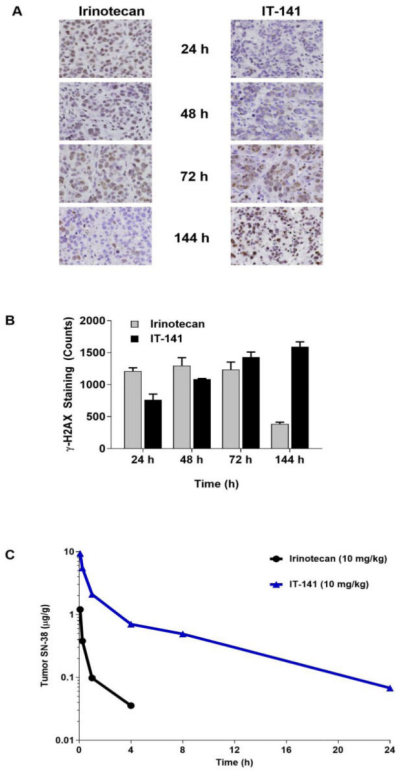

Figure 6.

Immunohistochemistry compares the pharmacodynamics effects of SN-38 in the tumor from irinotecan compared to delivery by IT-4 . (A) mmunohistochemical staining of γ-H2AX for the presence of DNA double stranded breaks at time points between 24-144 hours showing irinotecan treatment compared to IT-141 treatment in HT-29 colorectal tumor model. (B) Quantification of γ-H AX positive stained cells at same time points (n ≥ 2 tumors). Results represent means ± SEM. * $P < 0.05$, ** $P < 0.01$, *** $P < 0.001$. (C) Intravenous administration of IT-141 results in more than a 10-fold exposure of SN-38 over irinotecan to the tumor compartment. IT-141 had an SN-38 exposure of ($AUC_{0\text{-}24hrs}$) 7.2 compared to 0.65 of SN-38 following irinotecan administration.

Table 1

Characterization of micelle formulations encapsulating different APIs.

API	Avg. Diameter (nm)	Efficiency (%)	Drug Weight Loading (% wt/wt[1])	Dialysis > CMC (% remaining)	Dialysis < CMC (% remaining)
Aminopterin	70	68	5.0	75	65
Daunorubicin	58	82	7.2	95	61
Epothilone D	75	91	4.4	94	68
Paclitaxel	72	65	3.0	91	77
Panobinostat	80	88	7.4	95	93
SN-38	120	90	3.8	--	--

[1] % wt drug/wt polymer

Table 2

Efficacy results in colorectal (HT-29, HCT116) and lung (NCI-H460, A549) models treated with IT-141 or IT-147.

Tumor	Treatment	% TGI	Fold Change
HT-29	Formulation Control	-	4.8
	IT-141 (40 mg/kg)	64%	2.4
	IT-141 (60 mg/kg)	98%	1.1
HCT116	Formulation Control	-	9.7
	Irinotecan	70%	3.6
	IT-141 (50 mg/kg)	106%	0.5
NCI-H460	Formulation Control	-	11.0
	Epothilone D	23%	8.8
	IT-147 (30 mg/kg)	40%	7.1
A549	Formulation Control	-	2.2
	Epothilone D	2%	2.2
	IT-147 (30 mg/kg)	46%	1.6
HCT116	Formulation Control	-	8.6
	Epothilone D	38%	5.7
	IT-147 (30 mg/kg)	87%	2.0